INL/CON-09-16896
PREPRINT

Analysis of Developing Gas/Liquid Two-Phase Flows

ICMF 2010

Elena A. Tselishcheva
Michael Z. Podowski
Steven P. Antal
Donna Post Guillen
Matthias Beyer
Dirk Lucas

June 2010

The INL is a
U.S. Department of Energy
National Laboratory
operated by
Battelle Energy Alliance

Analysis of Developing Gas/Liquid Two-Phase Flows

Elena A. Tselishcheva*, Michael Z. Podowski*, Steven P. Antal*
Donna Post Guillen†, Matthias Beyer‡, Dirk Lucas‡

(*) Center for Multiphase Research, MANE Department, Rensselaer Polytechnic Institute, Troy, NY 12180 USA

(†) Idaho National Laboratory Idaho Falls, ID 83415, USA

(‡) Forschungszentrum Dresden-Rossendorf e.V. Institute of Safety Research, Dresden, Germany

tselie@rpi.edu, podowm@rpi.edu, antals@rpi.edu, Donna.Guillen@inl.gov, M.Beyer@fzd.de, d.lucas@fzd.de

Keywords: developing gas/liquid two-phase flow, Computational Multiphase Fluid Dynamics, bubbly and churn-turbulent flow regimes, NPHASE-CMFD code

Abstract

The objective of this work has been to study the mechanisms governing flow and phase distributions in developing gas/liquid two phase flows in general, and the evolution of different size bubbles in an adiabatic vertical pipe in particular. Flow regimes from bubbly to churn-turbulent have been accounted for. The main emphasis of the work has been on the modeling of various interfacial forces between the dispersed bubbles and the continuous liquid, as well as of bubble/bubble interactions (coalescence and breakup).

The proposed modeling concept uses a complete set of transport equations for each field, such as the continuous liquid and dispersed bubble fields. The overall model has been implemented in a state-of-the-art computational multiphase fluid dynamics code, NPHASE–CMFD. This three-dimensional four-field model, including the continuous liquid field and three dispersed gas fields representing bubbles of different sizes, has been carefully tested for numerical convergence and accuracy, and then validated against the TOPFLOW experimental results.

The NPHASE-CMFD simulations were aimed at demonstrating the capability of the proposed modeling concepts to predict the evolution of bubble concentration from channel inlet to near-equilibrium (fully-developed) conditions downstream. Along with several interfacial closure laws, the effect of elevation on air density has also been included in the model.

Introduction

Computational Multiphase Fluid Dynamics (CMFD) has become a very useful tool for the analysis and design optimization of a large class of multicomponent flow systems. However, the accuracy of numerical predictions for gas/liquid two-phase flows using CMFD methods strongly depends on the proper formulation of models governing the underlying local physical phenomena.

The purpose of this project has been to develop, test and validate a multifield model of adiabatic gas/liquid flows at intermediate gas concentrations (e.g., bubbly and churn-turbulent flow regimes), in which multiple-size bubbles are divided into a specified number of groups, each representing a prescribed range of sizes. In particular, the ability of the proposed modeling concept has been investigated to predict the evolution of bubble concentration from channel inlet to near-equilibrium (fully-developed) conditions downstream along an adiabatic vertical pipe.

The simulations were performed using a state-of-the-art computational multiphase fluid dynamics code, NPHASE–CMFD (Antal et al., 2000). A complete four-field model, including the continuous liquid field and three dispersed gas fields representing bubbles of different sizes, was first carefully tested for numerical convergence and accuracy, and then used to reproduce the TOPFLOW experimental data (Prasser et al, 2007).

Nomenclature

i,j,k	Numerical indexes
j	Superficial velocity (ms^{-1})
L	Length (m)
P	Pressure (Pa)
v	Velocity vector (ms^{-1})
x,y,z	Coordinates
m'''	Volumetric mass transfer between fields representing the same phase
M	Interfacial force per unit volume (Nm^{-3})
g	Acceleration of gravitation (ms^{-2})

A''' Interfacial area density (m^{-1})
u_{rel} Relative velocity of the dispersed field (m s^{-1})
Re Reynolds Number
D Diameter (m)
D_b Diameter of bubble (mm)
C_D Drag force coefficient
C_L Lift force coefficient
C_W Wall force coefficient
C_{TD} Turbulent dispersion coefficient
k Turbulent kinetic energy (m^2s^{-2})
K_{ij} Measure of the probability of coalescence or breakup
P_c Shear production rate
P_{ij} Relative probability of coalescence
Re_b Bubble relative Reynolds number
f_{ij} Frequency of collisions
y_w Distance from the wall (m)

Greek letters

α Volumetric gas fraction
μ Dynamic viscosity (kg $m^{-1}s^{-1}$)
τ Shear stress (kg $m^{-1}s^{-2}$)
ρ Density (kg m^{-3})
ν Kinematic viscosity (m^2s^{-1})
ε Turbulent dissipation rate (m^2s^{-3})
η_{kj} Measure of the effect of departure of large bubbles' shape from spherical
σ Surface tension

Subscripts

l,v Indexes for liquid and gas respectively
t Turbulent
b Bubble

Model formulation for churn-turbulent flows

The multifield modeling concept of multiphase/ multicomponent flows is based on ensemble averaging the governing equations for each component fluid. Such modeling, with appropriate closure laws, is capable of capturing flow regimes from bubbly through churn-turbulent and slug, to annular flow. A typical form of the resultant conservation equations for adiabatic flows is shown below.

Mass conservation

$$\frac{\partial(\alpha_k\rho_k)}{\partial t}+\nabla\cdot(\alpha_k\rho_k\mathbf{v}_k)=\dot{m}_k''' \tag{1}$$

Momentum conservation

$$\frac{\partial(\alpha_k\rho_k\mathbf{v}_k)}{\partial t}+\nabla\cdot(\alpha_k\rho_k\mathbf{v}_k\mathbf{v}_k)= -\alpha_k\nabla p_k+\nabla\cdot(\alpha_k\underline{\underline{\tau}}_k)+\alpha_k\rho_k\mathbf{g}+\sum_j\mathbf{M}_{kj}^i+\sum_m\dot{m}_{m,k}'''\mathbf{v}_m^i \tag{2}$$

where $\dot{m}_k'''=\sum_m\dot{m}_{m,k}'''$.

In Eqs.(1) and (2), α_k is the volumetric fraction of field-k, $\dot{m}_k'''$ is the volumetric mass transfer term into field-k from other fields representing the same phase, $\mathbf{M}_{kj}^i$ is the interfacial momentum transfer per unit time (interfacial force) between fields k and j, $\underline{\underline{\tau}}_k=\underline{\underline{\tau}}_k^{\mu}+\underline{\underline{\tau}}_k^{\mathrm{Re}}$ is the total shear stress term, the subscript 'i' refers to interfacial variables, and the remaining notation is conventional.

The interfacial interactions between the individual bubble fields are specified by mechanistic models for both drag and non drag forces. The total interfacial force on phase-k can be expressed as a superposition of several component forces (Drew, 1992):

$$\mathbf{M}_{l-v}^i=\mathbf{M}_{l-v}^D+\mathbf{M}_{l-v}^{VM}+\mathbf{M}_{l-v}^{TD}+\mathbf{M}_{l-v}^L+\mathbf{M}_{l-v}^W \tag{3}$$

where $\mathbf{M}_k^D$ is the drag force, $\mathbf{M}_k^{VM}$ is the virtual mass force, $\mathbf{M}_k^{TD}$ is the turbulent dispersion force, $\mathbf{M}_k^L$ is the lift force and $\mathbf{M}_k^W$ is the wall force.

Numerous closure laws can be found in literature to model the various interfacial forces, usually based on theoretical or experimental studies on single bubble. In the axial direction, the drag force and virtual mass force (Drew, 1992) play major roles. The drag force model is given by

$$\mathbf{M}_{l-v}^D=-\frac{1}{8}C_D|\mathbf{v}_v-\mathbf{v}_l|(\mathbf{v}_v-\mathbf{v}_l)A''' \tag{4}$$

Several models have been developed for the flow regime dependent drag coefficient, C_D. In the present study, the expression proposed by Wallis (1976) has been used

$$C_D=\begin{cases}\frac{24}{Re_b}\left[1+0.1Re_b^{0.75}\right] & for\ Re_b\le 1000\\ 0.44 & for\ Re_b>1000\end{cases} \tag{5}$$

where Re_b is the bubble Reynolds number relative to the surrounding it liquid

$$Re_b=\frac{|\mathrm{v}_{rel}|D_b}{\mathrm{v}_l} \tag{6}$$

In the radial direction, the non-drag interfacial forces are dominant and control the gas profile. One of them is the turbulent dispersion force. For small bubbles, this force can be evaluated from the model proposed by Podowski (2009). The radial component of this force is

$$\mathbf{M}_{l-v}^{TD}=C_{TD}\rho_l\alpha\nabla\left[(1-\alpha)\overline{\mathbf{v}'_c\,\mathbf{v}'_c}\right] =-C_{TD}\rho_l\alpha\overline{\mathbf{v}'_c\,\mathbf{v}'_c}\nabla\alpha+C_{TD}\rho_l\alpha(1-\alpha)\nabla\left[\overline{\mathbf{v}'_c\,\mathbf{v}'_c}\right] \tag{7}$$

where for isotropic turbulence, $C_{TD}=2/3$.

The first term of the RHS of Eq.(7) is normally dominant across most of the flow area, except for the near-wall region. In the latter region, the magnitude of the second term is significantly higher. Thus, the second term plays in fact the role of a wall force, preventing small bubbles from touching the wall.

For large bubbles, the turbulent dispersion force in the radial direction can obtained from

$$\mathbf{M}_{l-v}^{TD}=-C_{TD}\rho_l\alpha\nabla\alpha \tag{8}$$

The use of different formulations for different bubble sizes (and also different values of the coefficient, C_{TD}) is due to the fact that the force on large bubbles is caused by bubble-induced turbulence rather than by the micro-scale turbulence inside the liquid-field.

The lift force is used to account for the interfacial momentum exchange between bubbles and the liquid field. In the radial direction, this force can be written as

$$\mathbf{M}_{l-v}^L=-C_L\rho_l\alpha(\bar{\mathbf{v}}_v-\bar{\mathbf{v}}_l)\times(\nabla\times\bar{\mathbf{v}}_l) \tag{9}$$

For turbulent two-phase flows, this coefficient is typically between 0.03 and 0.1. However, for large non-spherical bubbles, the lift coefficient can not only reduce all the way

to zero, but even change sign. The critical diameter at which the lift coefficient changes sign has been estimated at 4 mm by Kurul and Podowski (1988) and at 5.8 mm by Tomiyama (1998).

Also, for large bubbles the alternate approach to model the effect of wall force has been used in the form of a lubrication force

$$\mathbf{M}_{l-v}^{W} = -C_W \rho_l \alpha \frac{|\mathbf{v}_v - \mathbf{v}_l|^2}{D_b} \mathbf{n}_w \tag{10}$$

where the wall force coefficient, C_W, is (Antal, 2005)

$$C_W = \begin{cases} C\left[1 + \left(\frac{y_w}{D_b}\right)^2 (2\frac{y_w}{D_b} - 3)\right] & \text{for } y < D_b \\ 0 & \text{for } y \geq D_b \end{cases} \tag{11}$$

In the present simulations, it has been assumed that three groups of bubbles of different diameters enter the flow channel. As soon as the bubbles start coalescing, new, larger than original, bubbles are formed. This in turn leads to the formation of a large spectrum of bubbles of different sizes. Eventually, the opposite process is also likely to occur, i.e. large deformed bubbles start breaking up, leaving behind small bubbles. Thus, it is very important that a mechanistic and accurate, yet computationally effective, mass transfer model be used to model the interactions between bubbles of different sizes (Kumbaro and Podowski, 2006). In the present model, the total volumetric mass transfer for field-*k* is defined as

$$m_k''' = m_{k,co}''' - m_{k,br}''' \tag{12}$$

where $m_{k,co}''' = \sum_m m_{m,k,co}'''$ is the rate of mass increase per unit volume of bubbles of group-*k* due to coalescence of bubbles of all groups, and $m_{k,br}''' = \sum_m m_{k,m,br}'''$ is the mass loss rate due to breakup of group-*k* bubbles into bubbles of different sizes.

A common approach of the modeling of bubble coalescence is based on a multiple-group concept. Specifically, if $D_{b,i}$ is the bubble diameter of bubble group-*i*, the rate of coalescence between bubbles of group-*i* and group-*j* is given in the form

$$m_{ij\to k}''' = K_{ij} \alpha_i \alpha_j \tag{13}$$

where K_{ij} is a measure of the probability of coalescence of two bubbles. Several models have been proposed to date for the coefficients, K_{ij}. The model used in current studies is defined as

$$K_{ij} = C_{ij-k} \rho_v f_{ij} P_{ij} \tag{14}$$

The group coefficients, C_{ij-k}, are the measures of probability that the coalescence of bubbles in group sizes *i* and *j* produce bubble of size-*k*. They can be determined using the modeling approach proposed by Podowski (2009), which is based on directly using a discrete combinatorial method.

The frequency of collisions is given by the following expression (Antal et al, 2005):

$$f_{ij-k} = \left[\frac{|\mathrm{v}_i - \mathrm{v}_l| d_i + |\mathrm{v}_j - \mathrm{v}_l| d_j}{\pi\left(d_i^2 + d_j^2\right)} + \delta_{ij} \frac{|\nabla \mathrm{v}_i|}{2\left(\alpha_{cr} - \alpha_i\right)^{1/3}} \right] \tag{15}$$

where

$$\delta_{ij} = \begin{cases} 1 & \text{if } i = j \\ 0 & \text{otherwise} \end{cases}$$

In Eq.(15), α_{cr} is the maximum concentration, or the critical packing limit, of small bubbles (α_{cr}=0.74 for spherical bubbles).

The relative probabilities of coalescence are normally estimated based on experimental observations. In general they decrease with the increasing bubble diameter (Prince and Blanch, 1990; Luo and Svendsen, 1996). A typical range for small bubbles can be estimated as

$$0.4 < P_{ij} < 0.8 \tag{16a}$$

whereas for small-to-large bubble coalescence we have

$$0.1 < P_{ij} < 0.4 \tag{16b}$$

The breakup of the large cap bubbles to form small bubbles can be expressed as:

$$m_{k-j}''' = K_{kj} \alpha_k = C_{k-ij} \rho_d f_{br,k-j} \alpha_k \tag{17}$$

It has been shown before that the volumetric mass transfer rate for large bubbles to form small bubbles depends mostly on the surface tension (Prince and Blanch, 1990; Luo and Svendsen, 1996). It is also influenced by the local turbulence level, and tends to increase with increasing energy dissipation rate. Taking into the account both factors, as well as the effects of the inertial and buoyancy forces, the following expression can be used for the frequency of large bubble breakup (Lehr et al, 2002)

$$f_{br,k-j} = \left(\frac{2\sigma}{\rho_l}\right)^{0.4} \left[\frac{6\eta_{kj} |\underline{\mathrm{v}}_k - \underline{\mathrm{v}}_l|^{0.2}}{\left(1 - \frac{\rho_d}{\rho_l}\right) D_k^{1.4} \left(\left(\frac{D_k}{D_j}\right)^3 - 1\right)} \right] \tag{18}$$

The group coefficients for break up model C_{k-ij} can be evaluated in a manner similar to that for the bubble coalescence model. The coefficient η_{kj} is a measure of the effect of departure of large bubbles' shape from spherical.

The effective viscosity of the continuous liquid field of the is given by

$$\nu_c^{\tau} = \nu_c + \nu_c^t + \nu_c^{2\phi} \tag{21}$$

where ν_c is the molecular kinematic viscosity of the liquid, $\nu_c^t = \frac{C_\mu k^2}{\varepsilon}$ is the turbulent shear-induced kinematic viscosity, and $\nu_c^{2\phi}$ is the bubble bubble-induced kinematic viscosity.

The turbulent shear-induced kinematic viscosity of the liquid component is modeled by a modified two-phase flow version of the High Reynolds Number *k-ε* model (Antal et al. 2005).

The bubble-induced kinematic viscosity is modeled using the following expression (Sato and Sekoguchi, 1975)

$$\nu_c^{2\phi} = \sum_{k=1}^{4} C_{\mu b} D_{b,k} \alpha_k \left| \underline{\mathrm{v}}_{d,k} - \underline{\mathrm{v}}_c \right| \tag{22}$$

where $C_{\mu b} = 1.2$.

Experimental Facility

The experimental data used for the validation of the present model have been taken at the thermal-dynamic test facility TOPFLOW (Prasser et al., 2007) at the Institute of Safety Research of Forschungszentrum Rossendorf e.V. The TOPFLOW facility has been equipped with a vertical test section, which is a stainless steel pipe with an inner diameter of 195.3 mm (DN200). The total height of the section is 9 m. The flow rates in the test section DN200 (see Fig.1) may be assigned over the following range: the superficial gas velocity (j_v) between 0.0025 and 7.772 m/s, and the superficial liquid velocity (j_l) from 0.0405 to 1.61 m/s. Desalinated water was used in the experiments. The metering system for the injected air flow supplied volumetric flow rates related to standard conditions (p=0.25MPa, T=30°C). The test section DN200 has been equipped with six gas injection locations which allowed for injecting air or steam via orifices in the pipe wall. This gas injection via wall orifices offers the advantage that the two-phase flow can raise smoothly to the measurement plane, without being influenced by the feeder within the tube at any other locations along the flow. The inlet part of the test section has been connected to a gas injection pipe and a compressed air system. The liquid phase has been supplied from the bottom of the test section. The measurement plane was always situated at the upper end of the test section shown in Fig. 1.

Two wire-mesh sensors were used. The lower sensor has been used to obtain data on gas volume fraction profiles and bubble size distributions, while the purpose of the second sensor was to determine gas velocity by cross-correlation measurements between the two sensors. Comparative measurements between the wire-mesh sensor and other research methods provided information on the accuracy of the measurement technique and the evaluation algorithms for the experimental determination of main flow parameters. The accuracy of the gas volume fraction averaged over the flow cross-section depends on the two-phase flow regime. Differences in the absolute void fraction were determined for bubbly flows in the range of ± 1 %, and a systematic underestimation of about - 4 % was observed for slug flows. The database established during the experiment contains data for the evolution of the flow along the pipe, including radial profiles of the void fraction and gas velocity, as well as bubble size distributions.

Overview of the NPHASE-CMFD Computer Code

The NPHASE-CMFD code (Antal et al, 2000) is a nominally pressure-based finite volume computational multiphase fluid dynamics (CMFD) flow solver. The individual conservation equations for mass, momentum and energy, are solved for each field, together with the equations for continuous field turbulence. The mixture and field continuity equations are solved in coupled and segregated (uncoupled) manner, using stationary coefficient linearization. The code is fully unstructured and can utilize second-order accurate convection and diffusion discretization. The technology used by the NPHASE-CMFD code is an ensemble averaged multifield model of two-phase or multiphase flows.

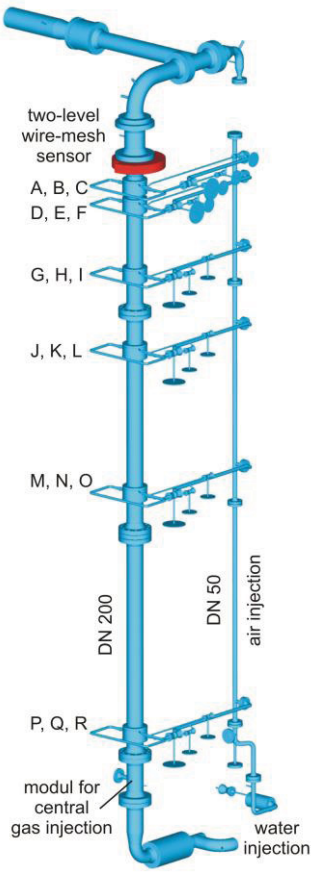

Figure 1. Vertical test section of the TOPFLOW facility with variable gas injection system (DN 200).

Key features of NPHASE-CMFD code include the following:

- Use of unstructured grids with arbitrary element types
- Capability to model an arbitrary number of fields (fluid components and/or phases)
- Built-in or user-defined mechanistic modeling, integrated with numerics
- Good robustness and numerical convergence
- Free surface modeling
- Parallel processing via MPI

Computational Grid and Boundary Conditions

The computational domain used in the NPHASE-CMFD simulations was consistent with the geometry of the TOPFLOW test section, and was shaped as a vertical circular tube, L= 9 m long and D = 0.194 m in diameter. A sample grid is shown in Figure 2. As it can be seen, nonuniform nodalization schemes have been used in both the radial and axial directions. Such an approach allowed one to capture flow details near the inlet, as well as the effect of high gradients of velocity and bubble concentration near the wall of the tube. GRIDGEN was used as a computational grid generator, to build the desired mesh and specify the necessary boundary conditions.

Table 1 presents the initial conditions used in testing and validation of the NPHASE-CMFD based model. These conditions correspond to the TOPFLOW experimental runs shown in the first column of Table 1.

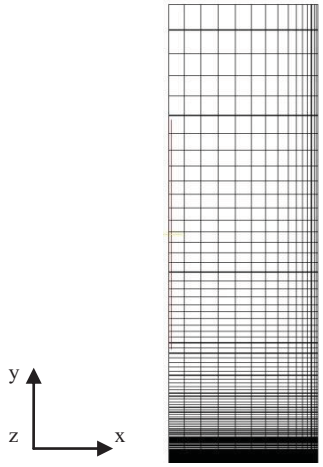

Figure 2. Schematic of grid geometry used in NPHASE-CMFD simulations.

Table 1. The initial conditions used in simulations

Run number	Superficial liquid velocity (m/s)	Superficial gas velocity (m/s)
107	1.017	0.145
118	1.017	0.219

Four groups of bubbles of different sizes have been identified in the TOPFLOW experiments. The majority of NPHASE-CMFD simulations have been performed for three bubble groups. This is because the measured concentrations of the two smallest bubble groups were very small (of the order of 3% or less), so that differentiating between them would be below the resolution level of the overall model.

The range of bubble sizes and the average bubble diameter for each modeled group were as follows:

Group-1: Size range from 0 to 5.8 mm; D_{b1} = 3 mm,

Group-2: Size range from 5.8 mm to 7 mm; D_{b2}= 6 mm,

Group-3: Size range over 7 mm; D_{b3}= 20 mm.

Parametric testing has shown that the differences between the results obtained using the integer values of bubble diameters given above and the arithmetic averages over each range were negligible.

During the experiment the temperature of the two-phase mixture in the TOPFLOW experiments was kept constant at 30°C. However, since the height of the experimental pipe was 9 m, the hydrostatic pressure drop between the inlet and the exit was comparable to the atmospheric pressure. This, in turn, has a significant effect on the density of the air, which decreased by nearly a factor of two compared to the initial density at a nearly atmospheric pressure. Thus, it was deemed important that this factor be accounted for in the model. Specifically, a position-dependent gas density has been assumed in the calculations, changing according to the ideal gas law

$$\rho_v(x) = (x_{out} - x)\frac{\rho_{v,in} - \rho_{v,out}}{L} + \rho_{v,out} \qquad (23)$$

where $\rho_{v,in} = \frac{p_{in}}{RT}$ is the air density at the inlet, $\rho_{v,out}$ is the air density at the pressure boundary (conduit's outlet), x_{out} is an axial coordinate of pressure boundary, x is the local axial coordinate, and $L = x_{out} - x_{in}$ is the total length of the conduit.

The inlet pressure was estimated based on the hydrostatic head of air/water mixture corresponding to the average void fraction observed in the experiments.

Results and discussion

Extensive testing of the proposed model has been performed using as a reference the experimental conditions corresponding to various data series of the TOPFLOW experiments (Prasser et al., 2007).

Several parametric simulations have been performed, in which the sensitivity of results to selected modeling assumptions has been assessed. The results included in the current paper show the parametric testing on the effects of gas density changes and of the values of selected interfacial force coefficients. The simulations have been performed for the liquid and gas flow rate corresponding to TOPFLOW Run 118.

To test the effect of gas density changes along the flow are shown in Figure 3, where the calculated axial distribution of gas density, along with the distributions of average void fraction, are plotted for the cases of variable and constant gas density. It can be seen that the average void fraction increases considerably with decreasing gas density, whereas it slightly decreases (due to gas acceleration) for a fixed gas density case. Thus, the changing (local-pressure deppendent) air density not only affects the magnitude of void fraction, but may also overcome the effect of buoyancy-driven bubble velocity increase.

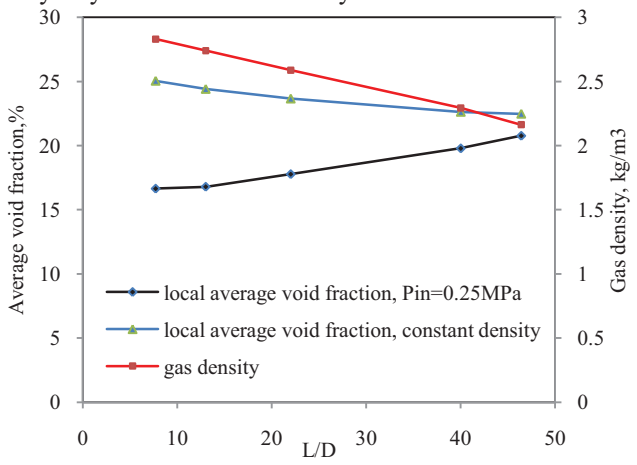

Figure 3. The effect of variable gas density on the average void fraction distribution along the TOPFLOW test section.

Figure 4 shows the effect of drag force on flow distribution. The Wallis correlation, discussed above, calculates the drag coefficient for small bubbles with a good accuracy. However, in the case of large bubbles, namely for Re>1000, its accuracy diminishes. The main reason is that it does not properly account for the effect of bubble deformation. As the bubble aspect ratio increases, the drag coefficient also increases. The diameter of large bubbles is still much smaller that the pipe diameter, so that those bubbles will maintain a near-ellipsoidal shape all the way along the flow. Several values of the drag coefficient

have been considered for test. They extend over the range from spherical bubbles to flat circular disks facing the flow (C_D=1.2). The present study has been performed for a two-field model of two-phase flow, consisting of a continuous liquid and large bubbles with D_b = 20 mm.

As it can be seen in Figure 4, bubble velocity decreases with increasing C_D, as expected. At the same time, there is an increase in the corresponding average void fraction. Interestingly, the void fraction distribution flattens as C_D increases. At the same time, the liquid velocity has not been affected by the value of drag coefficient. As a result of the present parametric testing, C_D=0.88 has been chosen as representative value of the drag coefficient for large bubbles for model validation purposes.

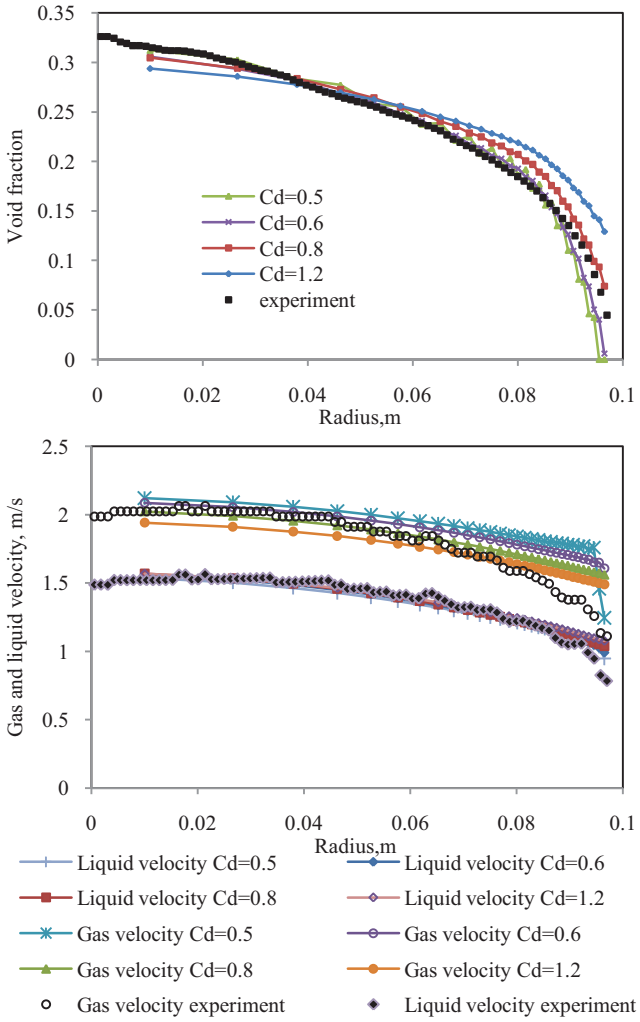

Figure 4. The effect of drag coefficient on the radial distributions of void fraction and phasic velocities. The calculated parameters correspond to a distance, L/D = 40 from pipe inlet; Run 118.

The experimental studies reported in literature on the effect of bubble deformation on the direction of lift force (Zun, 1980; Ervin & Tryggvason, 1997; Tomiyama, 1998) clearly show that the direction of this force changes if a substantial deformation of bubble shape occurs. Whereas small spherical bubbles typically travel toward the wall, large deformed bubbles behave in a different way. Namely, asymmetric deformations, caused by the combined effects of buoyancy and shear, lead to secondary flows around such bubbles, which change both the interfacial shear and pressure distribution around the bubble. This results in a change of direction of the lift force, compared to that for spherical bubbles. According to the observations of Tomiyama (1998), the critical bubble diameter at which lift force changes sign is approximately 5.8 mm for air/water flows at ambient conditions.

The impact of both the sign and magnitude on the radial distribution of large, 20 mm in diameter, bubbles and on the corresponding velocity profiles are shown in Figure 5.

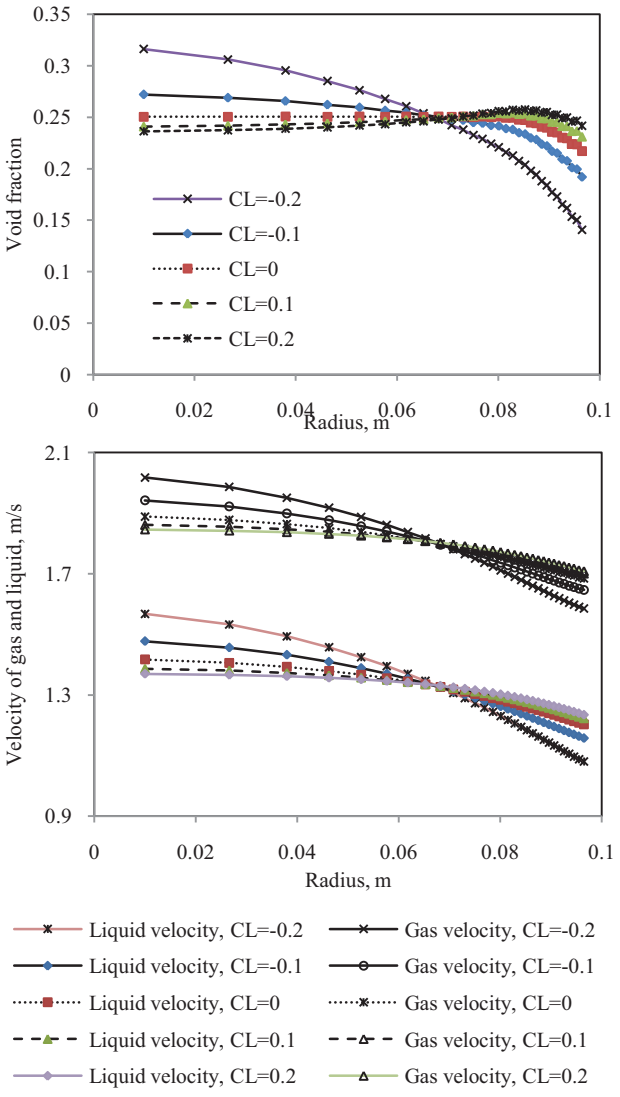

Figure 5. Radial void fraction and velocity profiles of large bubbles for different lift force coefficients. The calculated parameters correspond to a distance, L/D = 40 from pipe inlet; Run 118.

These results, which have been obtained for five different values of the lift coefficient, from C_L = 0.2 to C_L = -0.2, clearly demonstrate how the sign of lift coefficient affects bubble concentration. As expected, as the sign changes from positive to negative, the corresponding maximum value of the volume fraction has moved from the near the wall location to the center of the pipe.

The experimental data which have been used for the validation of the proposed complete multifield model of gas/liquid flows correspond to TOPFLOW Run 118 and

Run 107. In each simulation, the local gas and liquid velocity have been evaluated, along with the concentration distribution for each bubble group and the total void fraction. The radial profiles of those parameters have been plotted at different streamwise locations and compared against the experimental data.

Due the uncertainties associated with the effect of gas injection condition on flow conditions there, the measurements taken at two different distances (both short compared to the total pipe height) downstream from the injection zone have been used as inlet condition for NPHASE-CMFD simulations.

Figures 6 and 7 show the results for Run 118 obtain using the inlet conditions corresponding to the TOPFLOW data collected at the axial location, *L/D*=13 along the pipe. As it can be seen, the NPHASE results agree well with experiment. The velocity distributions in Figure 6 are consistent with data in the bulk region, while they are slightly overpredicted near the wall. This is because there is a swarm of small and intermediate bubbles near the wall which affect the velocity of both phases in that region.

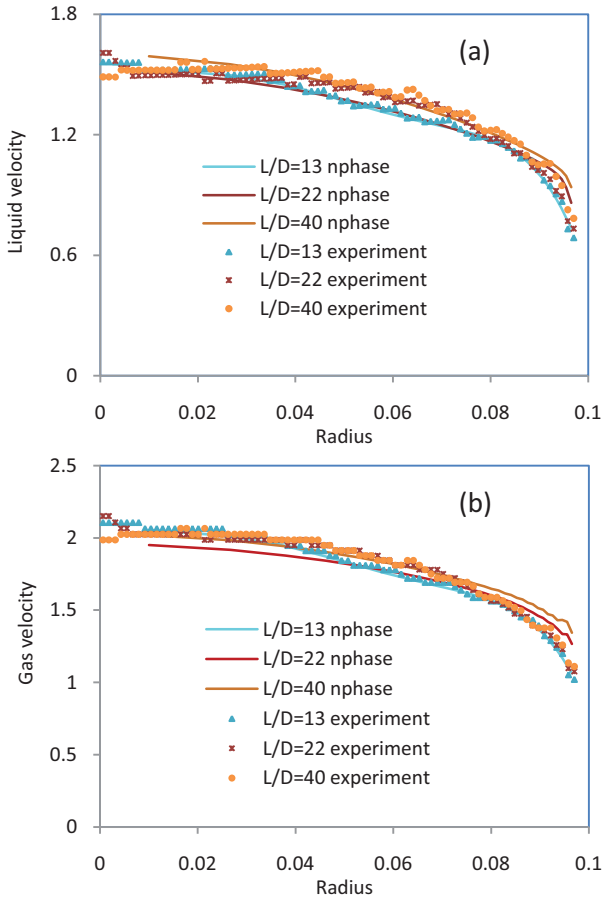

Figure 6. Evolution of a) liquid and b) gas velocity along the vertical channel for the case of four-field flow, compared against experimental data for Run 118. Starting point *L/D*=13.

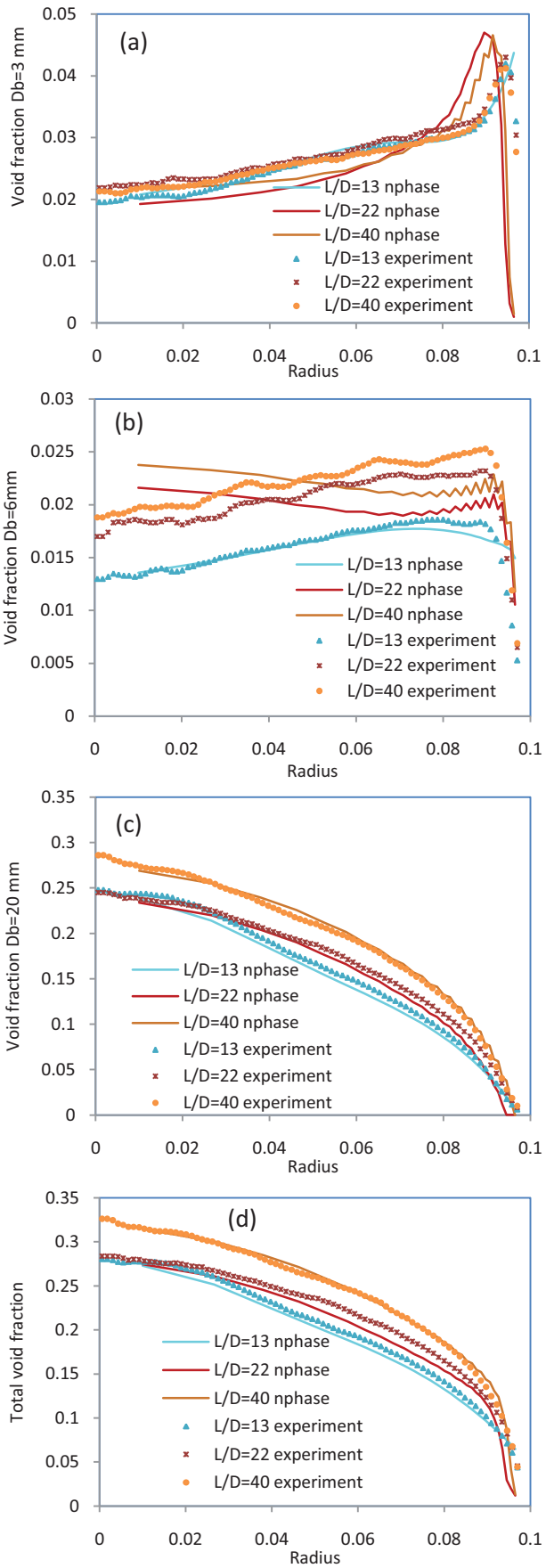

Figure 7. Evolution of concentration along the vertical channel for the case of four-field flow: a) D_b=3 mm; b) D_b=6 mm; c) D_b=20 mm; d) total void fraction. Run 118, starting point *L/D*=13.

Although the lift force for this bubble group is large enough to push the bubbles toward the wall, a small peak in the predicted distribution can still be observed near the center. On the other hand, the distribution of 3 mm diameter bubbles closely follows the experimental trend.

It is interesting to notice that the velocity profiles change only slightly along the flow between e, L/D=13 and L/D=40. The observed change in the gas concentration profiles is more significant in magnitude, but there have been no dramatic shape changes.

To better qualify the ability of the present model to predict two-phase flow parameter evolution in developing flows, a series of simulations has been performed using the axial location, L/D=7.7, as the starting point. The results of simulations are shown in Figures 8 and 9. As it can be seen, the volumetric concentration profile for small bubbles (D_B = 3 mm), shown in Figure 8(a) has been captured quite well, including the near-wall peak. The size of the intermediate group of bubbles (with D_B = 6 mm), belongs to the bubble diameter range for which the lift force changes direction, so concentration distribution in Figure 8(b) is nearly uniform, except for a slight peak near the wall. As shown in Figure 8(c), the agreement for large bubbles (D_B = 20 mm) is also very good, and the trend in the axial evolution of their radial concentration distribution has been captured in a consistent manner. Similar conclusions apply to the total void fraction distributions, shown in Figure 8(d). The results in Figure 9 indicate that a very good agreement with the data has also been obtained for the velocity distributions.

The evolution of the radial concentrations of different-size bubbles, as well as of the gas and liquid velocity magnitude profiles, are shown in Figure 10 for the entire computational domain. The left side of each color contour represents the wall boundary. The results in Figure 10 correspond to the same conditions as those shown in Figures 8 and 9. They allow one to better evaluate the developing flow characteristics along the channel. It can be seen that small bubbles stay near the wall all the way along the channel, while bubbles with a diameter of 6 mm are distributed uniformly along the pipe radius, with the maximum value of volumetric concentration around 3% near the outlet. At the same time, the large bubbles experience highest concentrations near the center of the pipe.

Since the previously discussed results have used a single TOPFOW run as a reference, it was deemed important that the new model be also validated against another set of flow conditions. Run 107 has been selected for this purpose, corresponding to the following flow conditions: j_l = 1.017 m/s, j_v = 0.14 m/s. These conditions also correspond to the churn-turbulent flow regime. Again, two series of simulations have been performed, one with the inlet conditions corresponding to L/D=13, the other to L/D=7.7. The results of simulations corresponding to the inlet conditions at L/D=13 are shown in Figures 11-12. The NPHASE-CMFD results again agree quite well with the experimental data.

Comparing the data for Run 107 (Fig. 11) with those for Run 118 (see Fig. 6), it can be observed that the profiles of void fraction for small and medium bubbles in the radial direction in Run 107 are nearly uniform (see Fig.11 (b)).

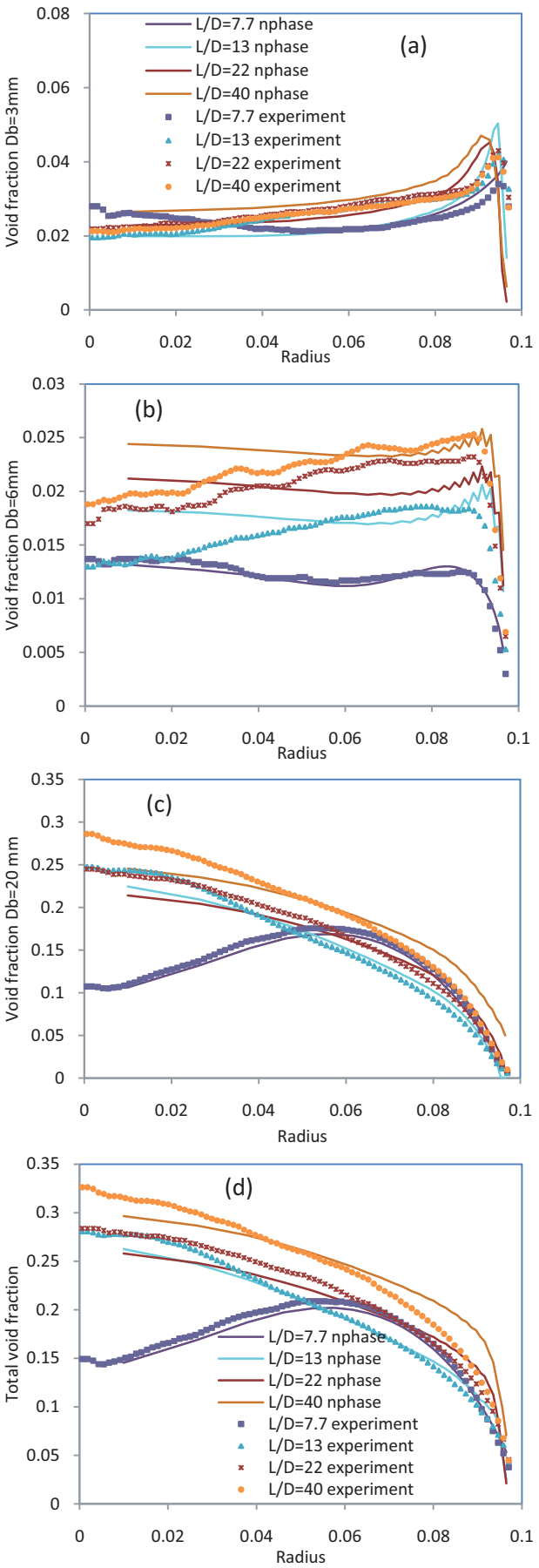

Figure 8. Evolution of concentration along the vertical channel for the case of four-field flow: a) D_b=3 mm; b) D_b=6 mm; c) D_b=20 mm; d) total void fraction. Run 118, starting point L/D=7.7.

Taking into account that the lift force coefficients for these bubbles are the same as in the previous simulations, the void fraction distributions of both small bubble groups has been captured relatively well, although the near-wall concentration of 3 mm diameter bubbles has been slightly overpredicted.

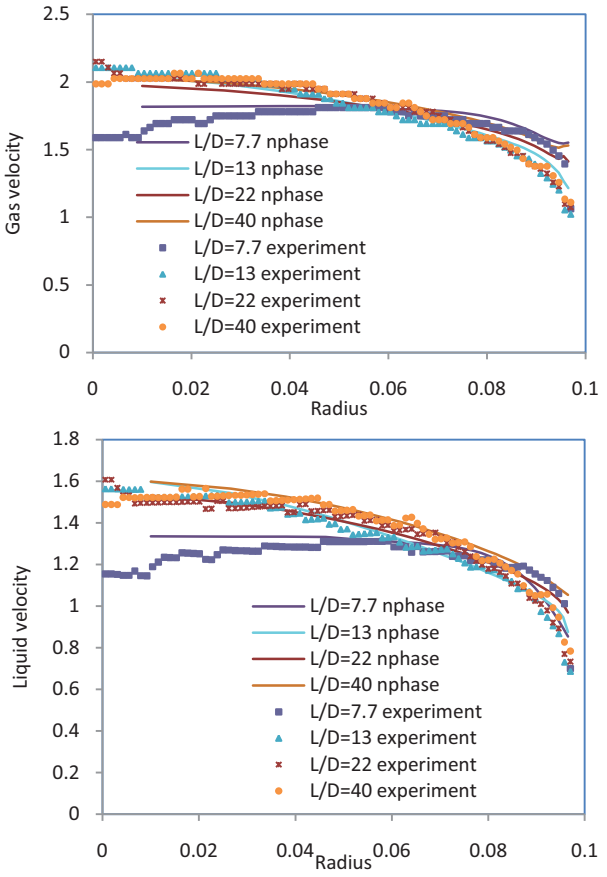

Figure 9. Evolution of flow velocity along the vertical channel for the case of four-field flow; Run 118, starting point L/D=7.7.

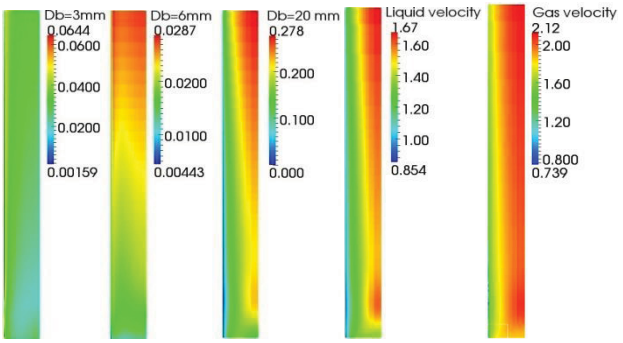

Figure 10. The side views of channel flow. The distributions of void fraction for each dispersed field, average gas and liquid velocities, Run 118.

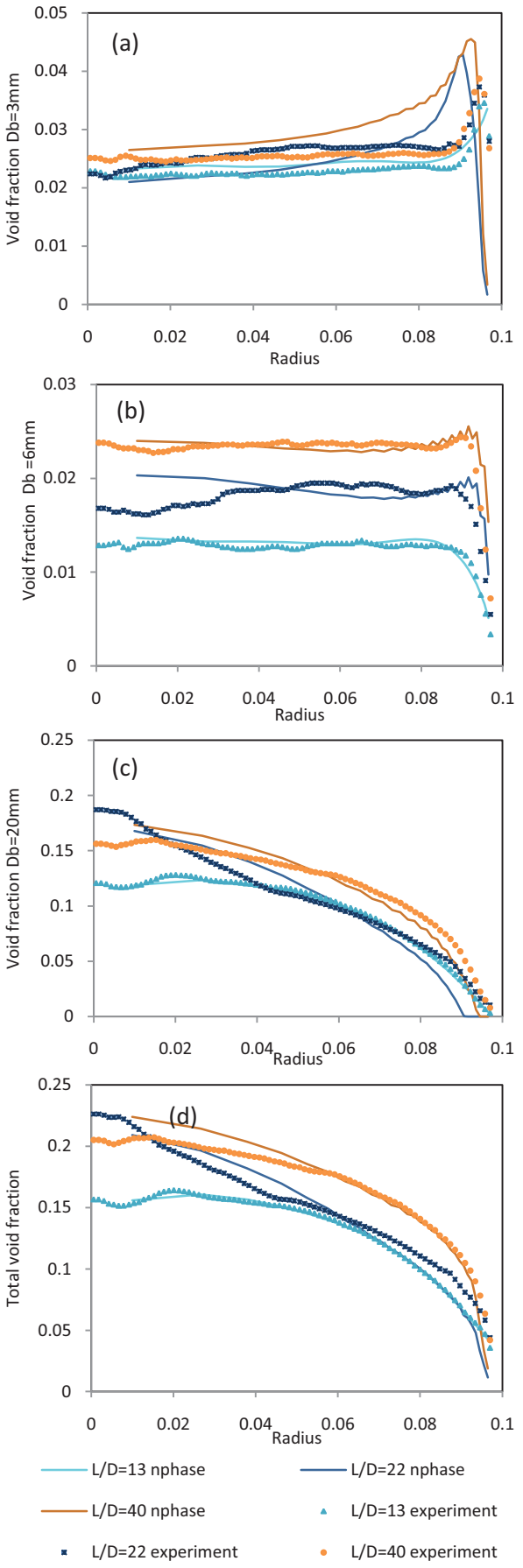

Figure 11. Evolution of concentration along the vertical channel for the case of four-field flow: a) D_b=3 mm; b) D_b=6 mm; c) D_b=20 mm; d) total void fraction. Run 107, starting point L/D=13.

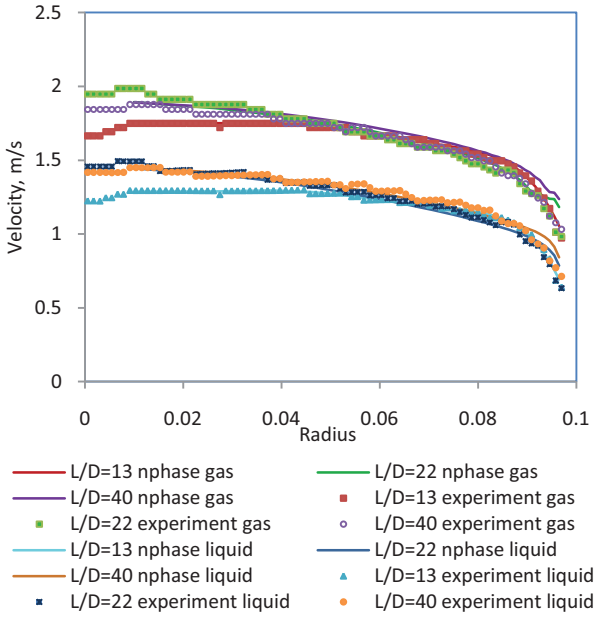

Figure 12. The development of velocity of liquid and gas along the channel. The comparison of radial distributions obtained by NPHASE against the experimental data for the Run 107, starting from L/D=13.

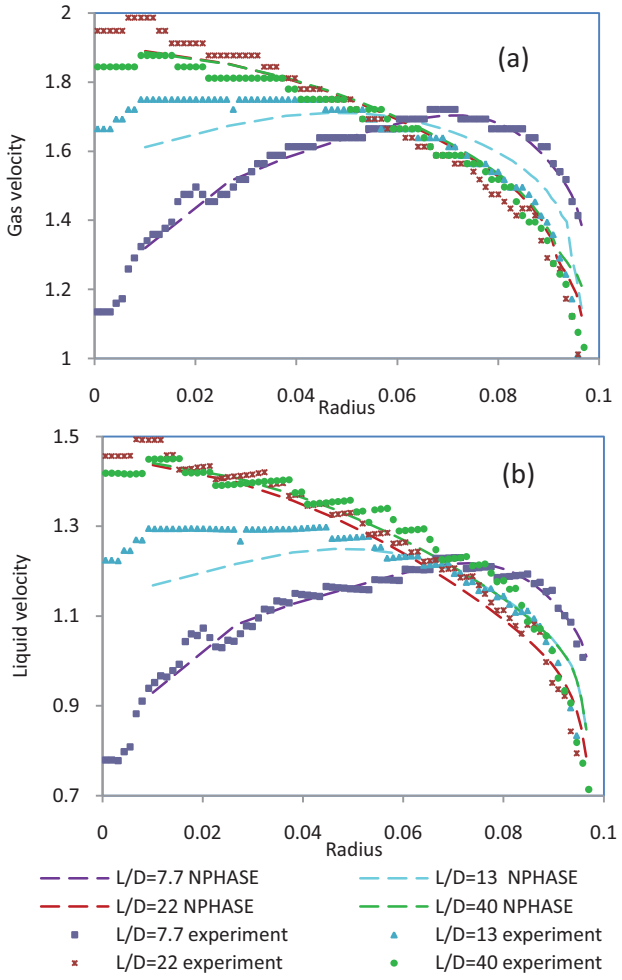

Figure 13. The development of velocity of a) gas and b) liquid along the channel. The comparison of radial distributions obtained by NPHASE against the experimental data for the Run 107. Starting point *L/D*=7.7.

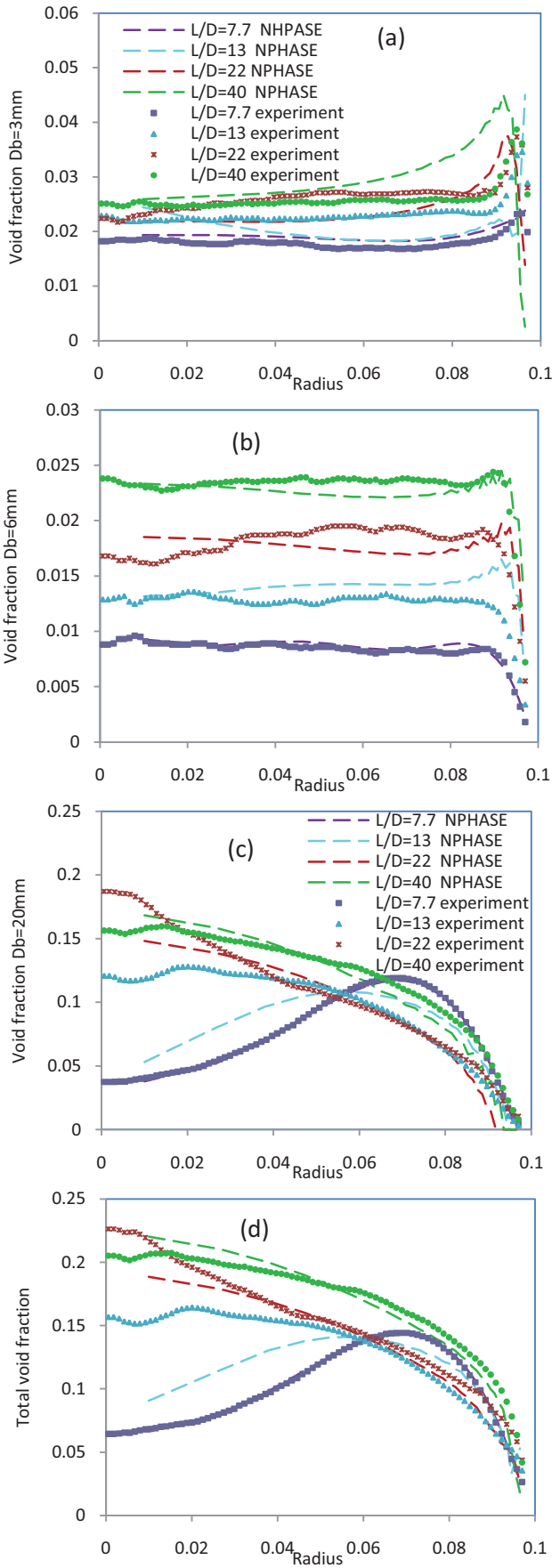

Figure 14. Evolution of concentration along the vertical channel for the case of four-field flow: a) D_b=3 mm; b) D_b=6 mm; c) D_b=20 mm; d) total void fraction. Run 107, starting point *L/D*=7.7.

The volume fraction distribution of large bubbles, as well as the total void fraction (see Fig.11 (d)), agree reasonably well with the data. The agreement between the predicted velocity profiles and the experimental measurements in Figure 12 is also quite good.

Figures 13 and 14 show again the results for TOPFLOW Run 107, but this time the experimental date at *L/D*=7.7 have been used at the inlet to the computational domain. As before, the results of predictions have been directly compared against the experimental data. Both the liquid and gas radial velocity profiles along the initial section of pipe, i.e. between *L/D*=7.7 and *L/D*=13, reach maximum values relatively close to the wall and then decrease toward the center of the pipe. Such velocity distributions affect the predicted concentration distribution of large bubbles at *L/D*=13, slowing down the transition to a center-peaked profile. The calculated concentration distributions for small and intermediate-size bubbles, shown in Figure 14, agree quite well with the data, although the center line concentration of large bubble at *L/D*=13 is underpredicted. In general, the results of NPHASE-CMFD predictions agree with the experimental trends along the flow, and they show good agreement at locations which are not too close to the gas inlet zone. The effect of geometry of the gas injection region on flow conditions and bubble distribution there, augmented by the experimental uncertainties, contribute to the modeling difficulties at distances close to this region.

Conclusions

The present work has achieved several objectives. One of them was to demonstrate the importance of proper physical closure modeling of two-phase flows in vertical conduits. In particular, selected computational and modeling issues have been investigated and resolved, associated with multidimensional simulations of multiphase flows using a multifield ensemble-averaged modeling framework. The overall model has been implemented in the NPHASE-CMFD solver and parametrically tested. The other major objective of this work was to demonstrate the ability of the NPHASE-CMFD code to predict the evolution of adiabatic churn-turbulent gas/liquid flows in vertical channels. The results of NPHASE-CMFD-based computer simulations confirm both the modeling and computational consistencies. The results of calculations have been compared with the several experimental data sets from the TOPFLOW test facility, and a good agreement has been observed.

Needless to say, several unresolved modeling and computational issues can still be identified, which require further investigation and additional future work. Among those are: the effect of interfacial forces on large deformed bubbles, the mass transfer model between bubbles of different sizes, and the mechanisms governing phase distribution evolution in developing flows.

Acknowledgments

Funding for this research was supported by the U.S. Department of Energy, Office of Nuclear Energy, under DOE Idaho Operations Office Contract DE-AC07-05ID14517. The experimental data were obtained at the Institute of Safety Research of Forschungszentrum Rossendorf e.V. in the frame of research project funded by the German Federal Ministry of Economics and Labor.

References

Antal, S.P., Ettorte, S.M., Kunz, R.F. and Podowski M.Z., Development of a next generation computer code for the prediction of multicomponent multiphase flows, Proc. Int. Conf. Trends in Num. and Phys. Modeling of Multiphase Flow, (2000)

Antal S.P., Podowski, M.Z., Lahey, R.T. Jr., Barber, D. and Delfino, C., Multidimensional Modeling of Developing Two-Phase Flows in a Large Adiabatic Riser Channel, Proceedings NURETH-11, Avignon, France, (2005)

Drew, D.A., Analytical modeling of multiphase flows, In Boiling Heat Transfer (Ed.: Lahey, R.T., Jr.), Elsevier, New York, (1992)

Ervin, E.A. and Tryggvason, G., The rise of bubbles in a vertical shear flow, Journal of Fluids Engineering, Vol. 119, (1997)

Kumbaro, A. and Podowski, M.Z., The effect of bubble/ bubble interactions on local void distribution in two-phase flows, Proceedings 13th International Heat Transfer Conference, Sydney, Australia, 2006.

Kurul, N. and Podowski, M.Z., Grid Generation for the Analysis of Dispersed Phase Motion in Two-Phase Flows, in Numerical Grid Generation in Computational Fluid Mechanics, Pineridge Press, (1988)

Lehr, F., Millies, M. and Mewes, D., Bubble Size Distributions and Flow Fields in Bubble Columns, AIChE Journal, Vol.48, (2002)

Luo, F. and Svendsen, H.F., Theoretical Model for Drop and Bubble Breakup in Turbulent Dispersions, AIChE Journal, Vol. 42, (1996)

Podowski, M.Z., On the consistency of mechanistic multidimensional modeling of gas/liquid two-phase flows, Nuclear Engineering and Design, Vol.239, 933–940, (2009)

Prasser, H.-M., Beyer, M., Carl, H., Manera, A., Pietruske, H. and Schutz, P., Experiments on upwards gas/liquid flow in vertical pipes, FZD-482, (2007).

Prince, M.J. and Blanch, H.W., Bubble Coalescence and Breakup in Air-Sparged Bubble Columns, AIChE Journal, Vol.36, (1990)

Sato, Y. and Sekoguchi, K., Liquid velocity distribution in two-phase bubble flow, Int. J. Multiphase Flow, Vol.2, (1975)

Tomiyama, A., Struggle with Computational Bubble Dynamics, Proceedings International Conference on Multiphase Flow, Lyon, France, (1998)

Wallis, G.B., One Dimensional Two Phase Flow, New York: Mc Graw-Hill, (1969)

Zun, I., The transverse migration of bubbles influenced by walls in vertical bubbly flow, International Journal of Multiphase Flow, Vol.6, (1980)